ADVANCING EARTH AND SPACE SCIENCES

JGR Space Physics

RESEARCH ARTICLE
10.1029/2024JA032419

Observation of Energetic Electron Near the Electron Diffusion Region of Magnetic Reconnection

Xiancai Yu[1], Quanming Lu[2,3], Rongsheng Wang[2,3], Xianguo Zhang[1], and Changbo Zhu[1]

[1]Beijing Key Laboratory of Space Environment Exploration, National Space Science Center, Chinese Academy of Sciences, Beijing, China, [2]Deep Space Exploration Laboratory/School of Earth and Space Sciences, University of Science and Technology of China, Hefei, China, [3]CAS Center for Excellence in Comparative Planetology/CAS Key Laboratory of Geospace Environment/Anhui Mengcheng National Geophysical Observatory, University of Science and Technology of China, Hefei, China

Key Points:

- Energetic electrons with energies up to 150 keV are observed near the electron diffusion region in Earth's magnetotail
- Low-energy electrons move mainly toward the X-line, while energetic electrons move mainly away from the X-line
- Non-thermal electrons (>6 kV) in these regions show power-law spectrum, indicating that the electrons have been accelerated efficiently

Correspondence to:

Q. Lu and X. Zhang,
qmlu@ustc.edu.cn;
zhangxg@nssc.ac.cn

Citation:

Yu, X., Lu, Q., Wang, R., Zhang, X., & Zhu, C. (2024). Observation of energetic electron near the electron diffusion region of magnetic reconnection. *Journal of Geophysical Research: Space Physics*, *129*, e2024JA032419. https://doi.org/10.1029/2024JA032419

Received 9 JAN 2024
Accepted 14 MAY 2024

Abstract Magnetic reconnection can effectively convert magnetic energy into plasma energy, and accelerate electrons. In this article, the electrons with energies up to 150 keV are observed in the separatrix region and near the electron diffusion region (EDR) detected by the Magnetospheric Multiscale mission in the magnetotail. Combined with the electron pitch-angle distribution, the electrons in these two regions have a striking behavior: the low-energy electrons (<∼10 keV) move mainly toward the X-line, while the energetic electrons (69–139 keV) move mainly away from the X-line. In the EDR, the energy of electrons can reach up to 10 keV and there is a notable enhancement in the flux of electrons in the direction perpendicular to the magnetic field, which implies the presence of acceleration processes occurring in the EDR, leading to the energization of electrons. Furthermore, the energy spectrum of non-thermal electron with energies above 6 keV shows a power law distribution in this event, suggesting the occurrence of multiple acceleration processes rather than a single energization mechanism. These findings underscore the EDR's role as a crucial region for electron acceleration during magnetic reconnection. The study provides essential clues about the mechanisms driving electron acceleration, contributing to our understanding of space weather phenomena and the broader dynamics of plasma physics in space environments.

1. Introduction

Energetic electrons are distributed widely in interplanetary space and are associated with many physical phenomena, for example, solar activities, magnetospheric substorms. Magnetic reconnection is one of the crucial mechanisms for the production of these energetic electrons. Previous studies found that a number of electrons can be directly accelerated to very high energy during magnetic reconnection (S. Y. Huang et al., 2012; Lin & Hudson, 1971; Q. Lu et al., 2022; Øieroset et al., 2001; Oka et al., 2023; Su et al., 2013; R. Wang et al., 2016; R. Wang, Lu, Li, et al., 2010). For example, energetic electrons of up to hundreds of keV have been detected in the vicinity of the reconnection region of the Earth's magnetosphere (L. J. Chen et al., 2008; H. S. Fu et al., 2013; Li et al., 2022; R. Wang, Lu, Li, et al., 2010). However, it is still outstanding issues that where and how these electrons are accelerated in reconnection.

After decades of efforts, a variety of acceleration mechanisms have been proposed. The microphysical processes in the electron diffusion region (EDR) are suggested to play an important role in particle acceleration (Burch et al., 2016; Z. Z. Chen et al., 2020; H. S. Fu et al., 2017; X. R. Fu et al., 2006; Li et al., 2022; Øieroset et al., 2002; Torbert et al., 2018; Xiong et al., 2022). In this region, the electron frozen-in condition is violated, namely the electrons are no longer coupled with the magnetic field, and a series of simulations have shown that the electrons can be accelerated by the reconnection electric field (X. R. Fu et al., 2006; C. Huang et al., 2010; Pritchett, 2006a, 2006b; Zelenyi et al., 1990) or via stochastic processes associated with turbulent structures near the reconnection X-line (S. Lu et al., 2020). However, there is still a serious lack of direct observational evidence for electron acceleration in the EDR (Ergun et al., 2018; Li et al., 2022). In addition, it has also been proposed that these electrons can be further accelerated in the reconnection exhaust region (Egedal et al., 2005, 2012; H. Fu et al., 2020; Hoshino, 2005; Hoshino et al., 2001; C. Huang et al., 2010; H. Wang et al., 2016; R. Wang et al., 2016), for example, parallel electric field acceleration in the separatrix region (SR) (Drake et al., 2005; Egedal et al., 2005, 2012; C. Huang et al., 2010; R. Wang et al., 2013, 2014; Yu et al., 2019; Yu, Lu, Wang, Gao, et al., 2021), the Fermi acceleration generated by the curvature drift (Dahlin et al., 2017; Drake et al., 2006; X. R.

Fu et al., 2006; H. Wang et al., 2016; R. Wang et al., 2016) and the Betatron acceleration generated by the gradient-B drift in the magnetic pick-up region (Dahlin et al., 2014; C. Huang et al., 2015, K. Huang et al., 2021).

In this article, we observed energetic electrons with energies up to 150 keV in the SR and the EDR boundary region of magnetotail reconnection. By examining the energetic electron energy and angular distributions, we enumerated the possible electron acceleration mechanisms and considered that EDR may be an important acceleration region for these energetic electrons. The remainder of this article was organized as follows: Section 2 illustrated the instrumentation and database. Section 3 presented an overview of the event. Finally, Section 4 presented the discussion and conclusions.

2. Instrumentation and Database

The burst mode data from several instruments onboard Magnetospheric Multiscale mission (MMS) were used in this paper. Three-dimensional (3D) magnetic field data with a cadence of 128 samples/s are measured by the Fluxgate Magnetometer (Russell et al., 2016). Electric field data with a cadence of 8,192 sample/s are taken from the Electric Double Probe (Ergun et al., 2016; Lindqvist et al., 2016). The plasma data are mainly obtained from the Fast Plasma Investigator (FPI) (Pollock et al., 2016), and FPI can provide the velocity-space distribution of electrons and ions from 10 eV to 30 keV with a time resolution of 30 and 150 ms, respectively. In this paper, the energy of electrons interested are up to 150 keV. The energy-angle distribution of energetic electrons (25–500 keV) at time resolution of <0.5 s is measured by the Fly's Eye Energetic Particle Sensor (Mauk et al., 2016). The data from MMS2 is used unless otherwise stated.

3. MMS Observations

At ∼22:33:18-22:34:20 UT on 11 July 2017, the MMS spacecraft was at around $[-21.6, 4.1, 3.8]R_E$ in the Geocentric Solar Magnetospheric coordinate system. Figure 1 presents the overview of the magnetic reconnection event, where all data are shown in the local current coordinates system with $\boldsymbol{L} = [0.9482, -0.2551, -0.1893]$, $\boldsymbol{M} = [0.1749, 0.9168, -0.3591]$, and $\boldsymbol{N} = [0.2651, 0.3074, 0.9139]$ GSM. In this coordinate system, the ion flow reversal (V_{iL}) coincides well with the magnetic field (B_N) reversal, consistent with the observational signatures of the spacecraft transiting the reconnection ion diffusion region. During this interval, MMS2 was always in the southern part of the current sheet ($B_L < 0$, shown in Figure 1b). When the ion flow V_{iL} reversed from tailward ($V_{iL} < 0$) to earthward ($V_{iL} > 0$) at around 22:34:02.6 UT (Figure 1c), the electron bulk flow displayed a similar overall reversal, and an enhancement of the electron bulk velocity in the out-of-plane direction V_{eM} was observed (Figure 1d), with a peak close to 20,000 km/s $\sim V_{Ae}$, where $V_{Ae} = B/\sqrt{\mu_0 n_e m_e}$ was the local electron Alfven velocity. It indicates that MMS2 satellite crossed the EDR from the tailward to the earthward, and more details have been described in previous studies (Torbert et al., 2018; Turner et al., 2021; Yu, Lu, Wang, Huang, et al., 2021).

In the tailward outflow region (∼22:33:18-22:34:00 UT), the ion velocity retained a high speed (∼−700 km/s) except for a short period (22:33:18-22:33:30 UT) when the ion velocity suddenly decreased to ∼−200 km/s, the electron flow V_{eL} changed sign from negative to positive, accompanied by a significant enhancement of the electric field perturbation, and B_L became a large value of −10 nT (Figure 1e). These observations meant that MMS2 crossed the SR in the tailward side of the X-line. The large positive B_M field was observed in tailward SR, which was consistent with the Hall magnetic field in the third quadrant of the quadrupolar field (Pritchett, 2001; Sonnerup, 1979; Terasawa, 1983). In this tailward SR, the electrons with positive velocity in the L direction ($V_{eL} > 0$) corresponds to the inflowing electrons, as described by Yu et al. (2019) and Yu, Lu, Wang, Gao, et al. (2021). Based on the above analysis, the satellite trajectory of MMS2 was displayed in Figure 1a, and the SR and EDR crossed by MMS were marked with blue and purple boxes, respectively. Remarkably, the enhancement of the electron flux with energy up to 150 keV were observed in the tailward SR (blue colorbar) and the boundary region of EDR (purple colorbar), as illustrated in Figure 1f.

Figure 2 shows the pitch-angle distributions of electrons in and around the EDR, and there are significant differences at different energies. During 22:34:00–22:34:02 UT, the electrons exhibited anti-sunward velocities (Figure 2b), and the corresponding magnetic field measurements were negative, reaching a minimum of −2.5 nT (Figure 2a), implying that MMS2 was located at the tailward boundary region of EDR. In this region, the electron parallel temperature can be up to ∼1,700 eV, much larger than its perpendicular temperature (Figure 2c).

Journal of Geophysical Research: Space Physics 10.1029/2024JA032419

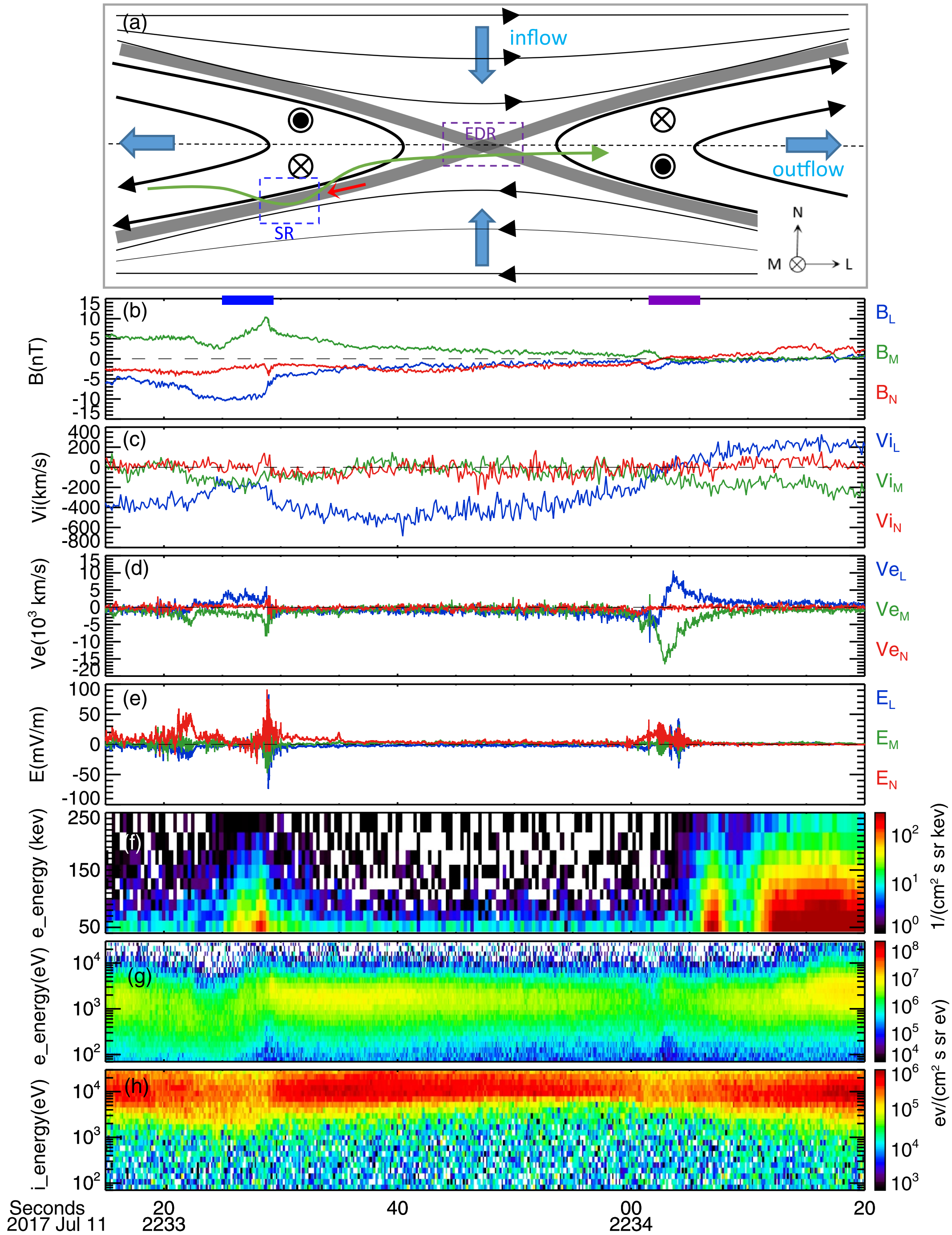

Figure 1. Overview of the magnetic reconnection. (a) Schematic illustrations for the reconnection diffusion region, where the blue and purple boxes represent the separatrix region and electron diffusion region crossed by Magnetospheric Multiscale mission. (b) Magnetic field components. (c) Ion velocity components. (d) Electron velocity components. (e) Electric field components. (f) Energetic electron (47–250 keV) omnidirectional differential flux. (g)–(h) Electron and ion energy spectrum, respectively.

Meanwhile, electrons with energies of 1–10 keV displayed a bi-directional distribution with a remarkable enhancement of the energy flux in the ~0° and ~180° directions (Figures 2f and 2g), and the energy flux in the parallel direction (~0°) was slightly greater than that in the anti-parallel direction(~180°). Combined with the local magnetic topology, the electrons with the pitch-angles of ~0° were moving toward the EDR, consistent with

10.1029/2024JA032419

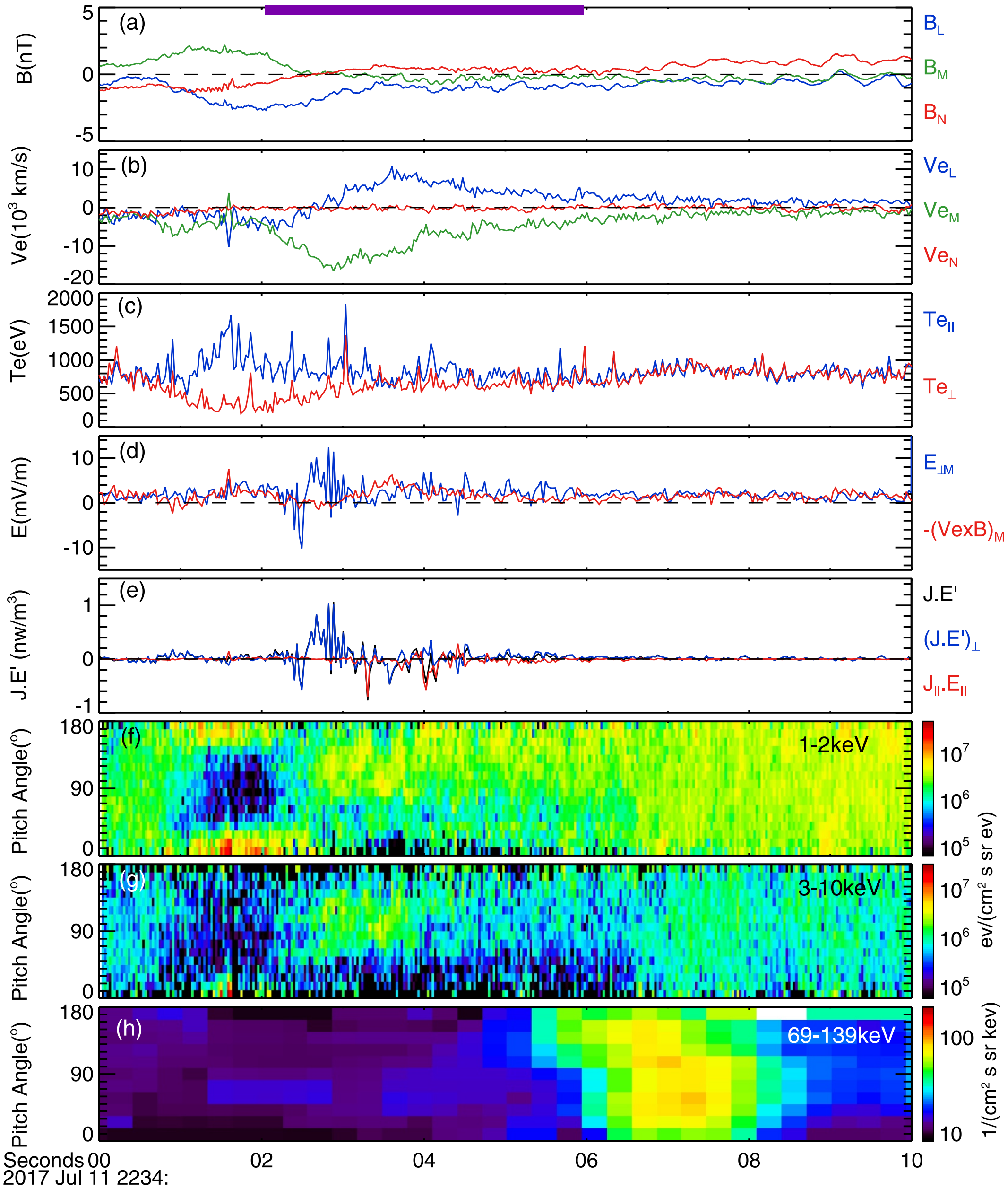

Figure 2. Observation of the electron distribution in/around the electron diffusion region (EDR). (a) Magnetic field components. (b) Electron velocity components. (c) Electron temperature. (d) The electric field $E_{\perp M}$ and $-(\mathbf{V_e} \times \mathbf{B})_M$. (e) The energy dissipation. (f)–(g) The electron pitch angle distribution with energies of 1–2 keV, 3–10 keV and 69–139 keV, respectively. The purple colorbar at the top represents the EDR.

previous observations and simulations of the SR (Q. Lu et al., 2010; Retinò et al., 2006; R. Wang et al., 2013, 2014).

During ~22:34:02-22:34:06 UT, the MMS entered the EDR with the reversal of the electron flow V_{eL} and magnetic field B_N, and the $-(\mathbf{V}_e \times \mathbf{B})_M$ was deviated from the measured electric field $E_{\perp M}$ (Figure 2d). In the EDR, the electron perpendicular temperature gradually increased and was comparable to its parallel temperature (Figure 2c). The energy dissipation $\mathbf{J} \cdot \mathrm{E}'$ was significantly enhanced and dominated by the perpendicular component $(\mathbf{J} \cdot \mathbf{E}')_\perp$ (Figure 2e), which can be up to ~1.0 nw/m^3. At the same time, the energy flux of electron with energies of 1–2 keV was enhanced between 90° and 180° (Figure 2f), and the energy flux of electron with energy of 3–10 keV was mainly concentrated in the perpendicular direction (Figure 2g). These observations suggested that the change of electron perpendicular energy dominates the energy enhancement process in the EDR (e.g., L.-J. Chen et al., 2016).

After 22:34:05 UT, MMS2 crossed the EDR into the earthward boundary region, where electron flow V_{eL} was positive (Figure 2b), and the pitch-angle distribution of electrons with energies of 1–10 keV gradually tended to be isotropic (Figures 2f and 2g). Distinctly, electrons with energies up to 150 keV were observed during 22:34:05-22:34:09 UT. The electron flux with energies of 69–139 keV was shown in Figure 2h, and it was enhanced in the antiparallel direction (∼180°) at ∼22:34:05 UT, and then gradually spread to other directions except ∼0°. Considering the local magnetic topology, it is inferred that the electrons with a pitch-angle of ∼180° located at the earthward boundary region of EDR were moving away from the EDR.

Figure 3 presents the characteristics of electrons in the tailward SR, highlighting notable differences in electron properties on each side of the separatrix. On the left side of the separatrix (22:33:25-22:33:28.8 UT), electrons exhibited positive velocities with the parallel velocity component prevailing, reaching speeds of approximately 10^4 km/s (Figure 3b). Concurrently, the electron parallel temperature increased significantly (Figure 3c), and the energy dissipation $\mathbf{J} \cdot \mathrm{E}'$ was positive, which was mainly contributed by the parallel component (Figure 3f). In this region, the energy flux of electron with energy of 2–10 keV was primarily intensified in the ∼180° direction (Figure 3g), consistent with the characteristics of the inflowing electrons within the SR. The synthesis of these observations suggested that the inflowing electrons were accelerated and heated in parallel directions, and a net positive parallel electric field, pointing away from the direction of EDR, was likely to facilitate the acceleration of these electrons in this region (Figure 3d). However, on the right side of the separatrix (22:33:28.8–22:33:30 UT), the electron velocity V_{eL} became negative (not shown), and the perpendicular component of electron velocity $V_{e\perp}$ increased (Figure 3b). Moreover, the pitch-angle distribution of electrons with energies of 2–10 keV exhibited a tendency toward isotropy (Figure 3g). Additionally, during 22:33:28.8–22:33:29.7 UT, the electron frozen-in condition was disrupted (Figure 3e), accompanied by significant energy dissipation $(\mathbf{J} \cdot \mathbf{E})'_{\perp}$ in the perpendicular direction (Figure 3f). The observation was consistent with the presence of non-ideal electric fields and energy dissipation within the SR reported with Yu et al. (2019), suggesting enhanced electron scattering and localized heating (Figure 3c).

The energetic electrons with energies up to 150 keV were also observed in this tailward SR. Figure 3h shows the electrons flux with energies of 63–139 keV in this region. Analysis of the pitch-angle distribution revealed an initial increase in the electron flux along the magnetic field lines (pitch angle ∼0°) at approximately 22:33:25 UT, and this flux then gradually broadened toward perpendicular direction (pitch angle ∼90°), with a notable spread at 22:33:28.5 UT. Given the magnetic topology within the tailward SR, it was possible to deduce that the energetic electrons, characterized by a pitch angle near 0°, were moving away from the EDR. This observation was consistent with the dynamics reported at the earthward boundary of the EDR, suggesting a commonality in the behavior of energetic electrons in these regions.

Notably, a complex magnetic structure was observed inside SR at ∼22:33:28.8 UT (marked by the vertical dotted line in Figure 3), which displayed a bipolar B_N diverging from the background magnetic field value of −3 nT, accompanied with a small peak of B_M (Figure 3a). This signature was consistent with a magnetic flux rope or Flux Transfer Event structure. For this magnetic structure, the center of the magnetic field reversal was precisely located on the separatrix, which divided regions with different electronic characteristics on either side. However, the spatial scale of the observed magnetic structure was significantly smaller than the distribution region of the energetic electrons. Consequently, it is still unclear whether this magnetic structure is related to the generation of energetic electrons in this region as observed previously (R. Wang et al., 2024; R. Wang, Lu, Du, & Wang, 2010).

Figure 4 shows the observed electron flux spectra of different regions in the reconnection diffusion region by the diamond symbols, including the EDR (black), the earthward boundary region of EDR (blue), the tailward SR (red) and the outflow region (green). The yellow dash-dotted line represents a Maxwellian distribution with a plasma density of 0.085 cm^{-3} and an electron temperature of 1 keV. It was clear that the electron distributions observed in all regions for energies greater than 6 keV exhibited deviations from the Maxwell distribution, suggesting the presence of non-thermal electrons. Above this energy threshold, the spectra align more closely with a power-law distribution of $f \propto E^{-\gamma}$, indicating that the electrons were accelerated multiple times. Due to the extremely low flux of electrons with energies greater than 30 keV in the EDR, only the distribution for energies between 6 and 30 keV in this region was fitted. The spectral indexes corresponding to each region were given at

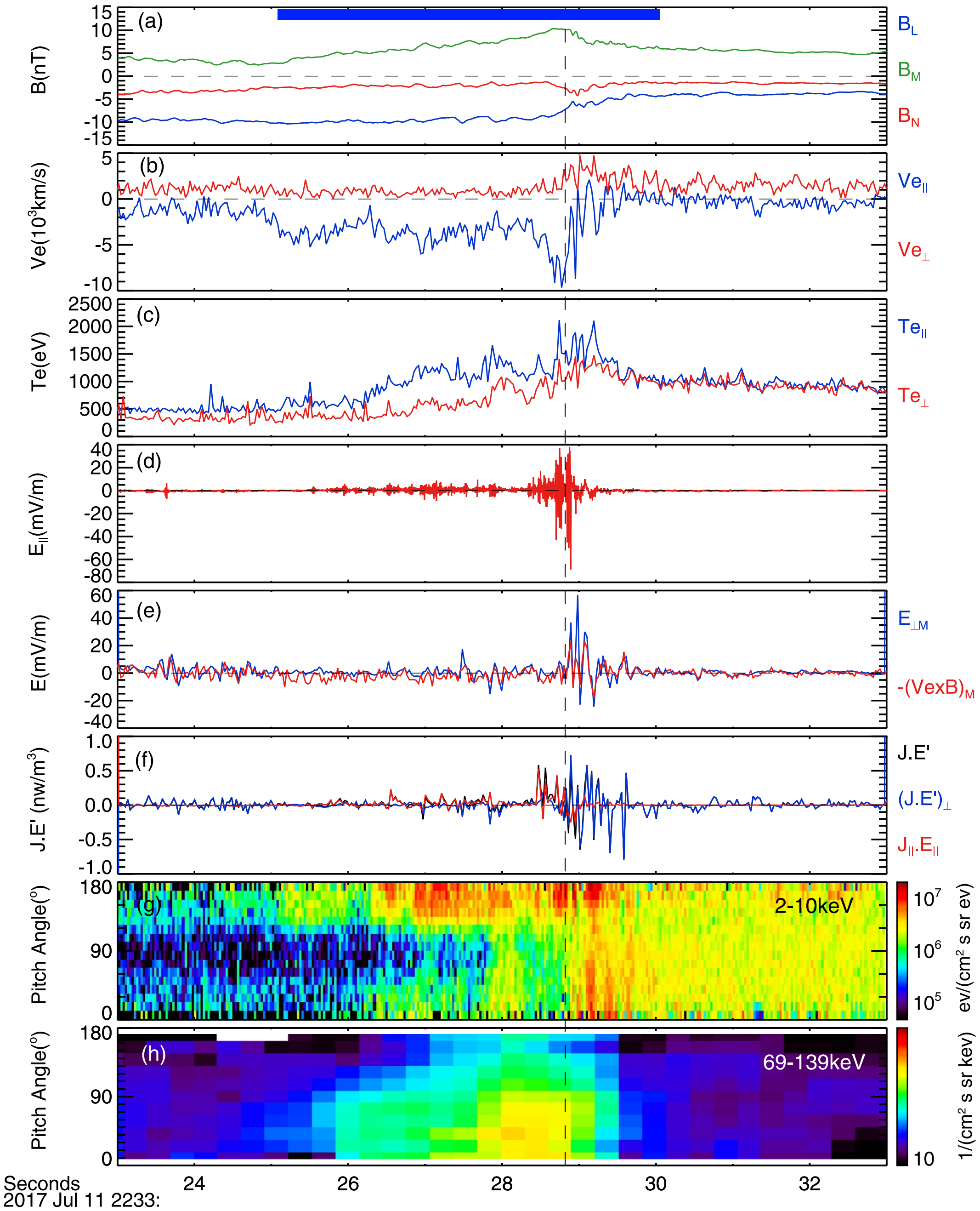

Figure 3. Observation of the electron distribution in the tailward separatrix region (SR). (a) Magnetic field components. (b) Electron velocity components. (c) Electron temperature. (d) The parallel electric field. (e) The electric field $E_{\perp M}$ and $-(\mathbf{V_e} \times \mathbf{B})_M$. (f) The energy dissipation. (g)–(h) The electron pitch angle distribution with energies of 2–10 keV and 69–139 keV, respectively. The blue colorbar at the top represents the SR.

the top of Figure 4. These measurements found that the power law index γ had an apparent local maximum (4.42) of the EDR region, with a trend of gradual hardening of the power-law index from the EDR region to the outflow region.

4. Discussion and Conclusions

In this article, we investigated the dynamics of energetic electrons in the magnetic reconnection focusing on electron populations with energies extending to 150 keV as detected in both the tailward SR and the earthward

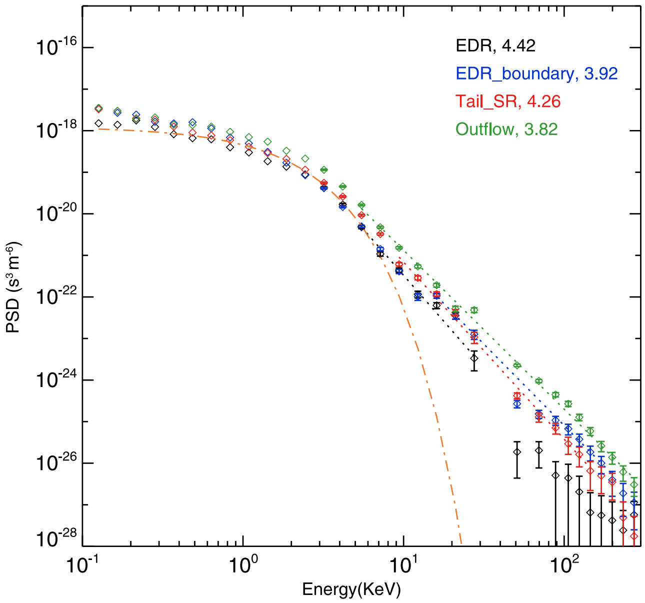

Figure 4. The electron energy spectrum at different reconnection region. The yellow dash-dotted line represents a Maxwellian distribution. The diamonds indicate the observed electron distribution, and the dotted lines are the fitted power law distributions, where blue indicates the boundary region of electron diffusion region (EDR), red represents the tailward separatrix region, Green is the outflow region, and black denotes the EDR. The spectral indexes are given in the upper right of the figure.

boundary of the EDR. Within the EDR region, electron energies have been observed to reach up to 10 keV. There was a notable increase in the electron flux at a 90° pitch angle, indicating that the electrons could be accelerated by the reconnection electric field in the EDR. Further analysis has shown that in the two regions where energetic electrons were detected, the pitch-angle distribution of electrons exhibited complexities that arose from the interactions of local magnetic and electric fields. The low-energy electrons (with energies of $< \sim 10$ keV) exhibited field-aligned distributions in the tailward SR and isotropic distributions in the earthward boundary of the EDR, with the field-aligned electrons in SR mainly moving toward the X-line, while the high-energy electrons (with energies of 69–139 keV) in these two regions exhibited field-aligned distributions that gradually spread out to the perpendicular direction, with the field-aligned electrons mainly moving away from the X-line. Therefore, we hypothesized that the energetic electrons observed in these two regions originated from the EDR, despite the lack of observed enhancement in electron flux within higher energy bands (greater than 30 keV) in the EDR. Given that the MMS satellite traversed only a very small portion of the EDR, it was plausible that it could miss regions where energetic electrons were present within the EDR.

Previous studies showed that the energy spectra can be represented by the power law distribution in the reconnection diffusion region (Cohen et al., 2021; X. R. Fu et al., 2006; Øieroset et al., 2002; Pritchett, 2006a). Øieroset et al. (2002) found that the fluxes of energetic electrons up to $\sim$300 keV peak near the center of the diffusion region, and the electron flux spectra obeys a power law with an index of 3.8 above $\sim$2 keV. Cohen et al. (2021) compared the spectral indexes of energetic (50–200 keV) electrons from six magnetotail EDR candidates encountered by MMS with those from "quiet-time" plasma sheet crossings, and found that EDR events tend to have a more significant population of energetic particles, corresponding to harder energy spectra with the spectral indexes typically in the range of 3–5, which provides evidence that the energetic electrons are in fact coming from the reconnection site. In our event, the non-thermal electrons in the EDR region exhibited a power law distribution with an index of about $\gamma \sim 4.42$, which was consistent with the observations of other EDR regions in Cohen et al. (2021) and further confirmed the importance of the EDR region for energetic electron generation in this event.

It remains unrevealed that how the energetic electrons are produced in such a limited EDR region. Many studies showed that the reconnection electric field plays an important for electron acceleration. Pritchett (2006a) suggested that the reconnection electric field can accelerate electrons to relativistic velocities via the two- and three-dimensional particle-in-cell simulations, which leads to an electron power-law spectrum with a slope of 5–6, comparable to our observations. However, it is still unclear that why the electrons can be trapped in the EDR for the persistent acceleration. The strong magnetic field in the SR and the weak magnetic field in the EDR can form a natural magnetic mirror type. Therefore, electrons can be trapped near the X-line and move back and forth along the magnetic field by the electrostatic potential (Egedal et al., 2005, 2008, 2012) and the magnetic mirror effect (R. Wang, Lu, Huang, & Wang, 2010). Subsequently, these electrons were trapped into the EDR, and undergone acceleration to gain energy by the reconnection electric field multiple times.

Recently, Li et al. (2022) observed energetic electrons up to 300 keV in the X-line region, although the non-thermal, power-law tail was soft with the power-law index of $\sim$8, and they found that the X-line region has evolved into turbulence with a complex filamentary current network. The results suggested that the non-ideal electric field in such filamentary current sheets can effectively accelerate electrons while the electrons were trapped in the filamentary current network. In our event, the electron current sheet observed by MMS for 2 s was still nearly laminar. Therefore, the electrons cannot stay in the EDR for a long time, which could be the reason why no energetic electrons were detected therein. Alternatively, MMS only passed the boundary of the whole EDR in this event and thus did not observe the energetic electrons which could have been created inside the EDR.

After ejected away from the EDR, the electrons could experience other acceleration processes. In this event, the presence of a parallel electric field in the SR pointing away from the EDR direction can provide a net parallel potential, and therefore lead to the flux enhancement along the magnetic field. In addition to the field-aligned flux enhancements, the high-energy electrons (69–139 keV) around the perpendicular directions relative to the magnetic field were observed in this event. The flux enhancements around the perpendicular directions were related to the increase of B_N both at the boundary of the EDR (~22:34:06.5-22:34:07.6 UT) and in the SR (~22:33:26-22:33:29 UT) and could be caused by the betatron acceleration at the so-called magnetic field pile-up regions (Hoshino et al., 2001). And the special magnetic structure existed in the tailward SR in this event, can also effectively trap electrons, leading to localized acceleration of electrons in the SR (S. Y. Huang et al., 2019).

In summary, these observations suggest that EDR is a critical region for electron acceleration during magnetic reconnection. Further study of these phenomena will help us to better understand the mechanisms and processes of electron acceleration during magnetic reconnection.

Data Availability Statement

All the MMS data used in this work are available at the MMS data center (https://lasp.colorado.edu/mms/sdc/public/about/browse-wrapper/). The data have been loaded, analyzed, and plotted using the SPEDAS software (Version 5.0) (Angelopoulos et al., 2019), which can be downloaded via the Downloads and Installation page (http://spedas.org/blog/).

Acknowledgments
Thanks to the MMS teams for the high-quality data and successful operation. This work was supported by Youth Innovation Promotion Association of Chinese Academy of Sciences (No. E3217A031S), and National Key Research and Development Program of China (No. 2022YFA1604600).

References

Angelopoulos, V., Cruce, P., Drozdov, A., Grimes, E. W., Hatzigeorgiu, N., King, D. A., et al. (2019). The space physics environment data analysis system (SPEDAS) (Version 5.0) [Software]. *Space Science Reviews*. https://doi.org/10.1007/s11214-018-0576-4

Burch, J. L., Torbert, R. B., Phan, T. D., Chen, L. J., Moore, T. E., Ergun, R. E., et al. (2016). Electron-scale measurements of magnetic reconnection in space. *Science*, *352*(6290), aaf2939. https://doi.org/10.1126/science.aaf2939

Chen, L. J., Bhattacharjee, A., Puhl-Quinn, P. A., Yang, H., Bessho, N., Imada, S., et al. (2008). Observation of energetic electrons within magnetic islands. *Nature Physics*, *4*(1), 19–23. https://doi.org/10.1038/nphys777

Chen, L.-J., Hesse, M., Wang, S., Bessho, N., & Daughton, W. (2016). Electron energization and structure of the diffusion region during asymmetric reconnection. *Geophysical Research Letters*, *43*(6), 2405–2412. https://doi.org/10.1002/2016gl068243

Chen, Z. Z., Wang, T. Y., Yu, Y., & Chen, F. (2020). Relationship between current filaments and turbulence during a turbulent reconnection. *The Astrophysical Journal*, *888*(2), L16. https://doi.org/10.3847/2041-8213/ab61fe

Cohen, I. J., Turner, D. L., Mauk, B. H., Bingham, S. T., Blake, J. B., Fennell, J. F., & Burch, J. L. (2021). Characteristics of energetic electrons near active magnetotail reconnection sites: Statistical evidence for local energization. *Geophysical Research Letters*, *48*(1), e2020GL090087. https://doi.org/10.1029/2020GL090087

Dahlin, J. T., Drake, J. F., & Swisdak, M. (2014). The mechanisms of electron heating and acceleration during magnetic reconnection. *Physics of Plasmas*, *21*(9), 092304. https://doi.org/10.1063/1.4894484

Dahlin, J. T., Drake, J. F., & Swisdak, M. (2017). The role of three-dimensional transport in driving enhanced electron acceleration during magnetic reconnection. *Physics of Plasmas*, *24*(9), 092110. https://doi.org/10.1063/1.4986211

Drake, J. F., Shay, M. A., Thongthai, W., & Swisdak, M. (2005). Production of energetic electrons during magnetic reconnection. *Physical Review Letters*, *94*(9), 095001. https://doi.org/10.1103/PhysRevLett.94.095001

Drake, J. F., Swisdak, M., Che, H., Shay, M. A., & Shay, M. A. (2006). Electron acceleration from contracting magnetic islands during reconnection. *Nature*, *443*(7110), 553–556. https://doi.org/10.1038/nature05116

Egedal, J., Daughton, W., & Le, A. (2012). Large-scale electron acceleration by parallel electric fields during magnetic reconnection. *Nature Physics*, *8*(4), 321–324. https://doi.org/10.1038/nphys2255

Egedal, J., Fox, W., Katz, N., Porkolab, M., Øieroset, M., Lin, R. P., et al. (2008). Evidence and theory for trapped electrons in guide field magnetotail reconnection. *Journal of Geophysical Research*, *113*(A12), A12207. https://doi.org/10.1029/2008JA013520

Egedal, J., Øieroset, M., Fox, W., & Lin, R. P. (2005). In situ discovery of an electrostatic potential, trapping electrons and mediating fast reconnection in the Earth's magnetotail. *Physical Review Letters*, *94*(2), 025006. https://doi.org/10.1103/PhysRevLett.94.025006

Ergun, R. E., Goodrich, K. A., Wilder, F. D., Ahmadi, N., Holmes, J. C., Eriksson, S., et al. (2018). Magnetic reconnection, turbulence, and particle acceleration: Observations in the Earth's magnetotail. *Geophysical Research Letters*, *45*(8), 3338–3347. https://doi.org/10.1002/2018GL076993

Ergun, R. E., Tucker, S., Westfall, J., Goodrich, K. A., Malaspina, D. M., Summers, D., et al. (2016). The axial double probe and fields signal processing for the MMS mission. *Space Science Reviews*, *199*(1–4), 167–188. https://doi.org/10.1007/s11214-014-0115-x

Fu, H., Grigorenko, E. E., Gabrielse, C., Liu, C., Lu, S., Hwang, K. J., et al. (2020). Magnetotail dipolarization fronts and particle acceleration: A review. *Science China Earth Sciences*, *63*(2), 235–256. https://doi.org/10.1007/s11430-019-9551-y

Fu, H. S., Khotyaintsev, Y. V., Vaivads, A., Retino, A., & Andre, M. (2013). Energetic electron acceleration by unsteady magnetic reconnection. *Nature Physics*, *9*(6), 426–430. https://doi.org/10.1038/nphys2664

Fu, H. S., Vaivads, A., Khotyaintsev, Y. V., André, M., Cao, J. B., Olshevsky, V., et al. (2017). Intermittent energy dissipation by turbulent reconnection. *Geophysical Research Letters*, *44*(1), 37–43. https://doi.org/10.1002/2016GL071787

Fu, X. R., Lu, Q. M., & Wang, S. (2006). The process of electron acceleration during collisionless magnetic reconnection. *Physics of Plasmas*, *13*(1), 012309. https://doi.org/10.1063/1.2164808

Hoshino, M. (2005). Electron surfing acceleration in magnetic reconnection. *Journal of Geophysical Research*, *110*(A10), A10215. https://doi.org/10.1029/2005JA011229

Hoshino, M., Mukai, T., Terasawa, T., & Shinohara, I. (2001). Suprathermal electron acceleration in magnetic reconnection. *Journal of Geophysical Research*, *106*(A11), 25979–25997. https://doi.org/10.1029/2001JA900052

Huang, C., Lu, Q., & Wang, S. (2010). The mechanisms of electron acceleration in antiparallel and guide field magnetic reconnection. *Physics of Plasmas*, *17*(7), 072306. https://doi.org/10.1063/1.3457930

Huang, C., Wu, M., Lu, Q., Wang, R., & Wang, S. (2015). Electron acceleration in the dipolarization front driven by magnetic reconnection. *Journal of Geophysical Research: Space Physics*, *120*(3), 1759–1765. https://doi.org/10.1002/2014JA020918

Huang, K., Lu, Q., Lu, S., Wang, R., & Wang, S. (2021). Formation of pancake, rolling-pin, and cigar distributions of energetic electrons at the dipolarization fronts (DFs) driven by magnetic reconnection: A two-dimensional particle-in-cell simulation. *Journal of Geophysical Research: Space Physics*, *126*(10), e2021JA029939. https://doi.org/10.1029/2021JA029939

Huang, S. Y., Jiang, K., Yuan, Z. G., Zhou, M., Sahraoui, F., Fu, H. S., et al. (2019). Observations of flux ropes with strong energy dissipation in the magnetotail. *Geophysical Research Letters*, *46*(2), 580–589. https://doi.org/10.1029/2018GL081099

Huang, S. Y., Vaivads, A., Khotyaintsev, Y. V., Zhou, M., Fu, H. S., Retinò, A., et al. (2012). Electron acceleration in the reconnection diffusion region: Cluster observations. *Geophysical Research Letters*, *39*(11), L11103. https://doi.org/10.1029/2012GL051946

Li, X., Wang, R., Lu, Q., Russell, C. T., Lu, S., Cohen, I. J., et al. (2022). Three-dimensional network of filamentary currents and super-thermal electrons during magnetotail magnetic reconnection. *Nature Communications*, *13*(1), 3241. https://doi.org/10.1038/s41467-022-31025-9

Lin, R. P., & Hudson, H. S. (1971). 10–100 keV electron acceleration and emission from solar flares. *Solar Physics*, *17*(2), 412–435. https://doi.org/10.1007/BF00150045

Lindqvist, P.-A., Olsson, G., Torbert, R. B., King, B., Granoff, M., Rau, D., et al. (2016). The spin-plane double probe electric field instrument for MMS. *Space Science Reviews*, *199*(1–4), 137–165. https://doi.org/10.1007/s11214-014-0116-9

Lu, Q., Fu, H., Wang, R., & Lu, S. (2022). Collisionless magnetic reconnection in the magnetosphere. *Chinese Physics B*, *31*(8), 089401. https://doi.org/10.1088/1674-1056/ac76ab

Lu, Q., Huang, C., Xie, J., Wang, R., Wu, M., Vaivads, A., & Wang, S. (2010). Features of separatrix regions in magnetic reconnection: Comparison of 2-D particle-in-cell simulations and Cluster observations. *Journal of Geophysical Research*, *115*(A11), A11208. https://doi.org/10.1029/2010JA015713

Lu, S., Artemyev, A. V., Angelopoulos, V., & Pritchett, P. L. (2020). Energetic electron acceleration by ion-scale magnetic islands in turbulent magnetic reconnection: Particle-in-cell simulations and ARTEMIS observations. *The Astrophysical Journal*, *896*(2), 105. https://doi.org/10.3847/1538-4357/ab908e

Mauk, B. H., Blake, J. B., Baker, D. N., Clemmons, J. H., Reeves, G. D., Spence, H. E., et al. (2016). The energetic particle detector (EPD) investigation and the energetic ion spectrometer (EIS) for the magnetospheric multiscale (MMS) mission. *Space Science Reviews*, *199*(1–4), 471–514. https://doi.org/10.1007/s11214-014-0055-5

Øieroset, M., Lin, R. P., Phan, T. D., Larson, D. E., & Bale, S. D. (2002). Evidence for electron acceleration up to ∼300 keV in the magnetic reconnection diffusion region of Earth's magnetotail. *Physical Review Letters*, *89*(19), 195001. https://doi.org/10.1103/PhysRevLett.89.195001

Øieroset, M., Phan, T. D., Fujimoto, M., Lin, R. P., & Lepping, R. P. (2001). In situ detection of collisionless reconnection in the Earth's magnetotail. *Nature*, *412*(6844), 414–417. https://doi.org/10.1038/35086520

Oka, M., Birn, J., Egedal, J., Guo, F., Ergun, R. E., Turner, D. L., et al. (2023). Particle acceleration by magnetic reconnection in geospace. *Space Science Reviews*, *219*(8), 75. https://doi.org/10.1007/s11214-023-01011-8

Pollock, C., Moore, T., Jacques, A., Burch, J., Gliese, U., Saito, Y., et al. (2016). Fast plasma investigation for magnetospheric multiscale. *Space Science Reviews*, *199*(1–4), 331–406. https://doi.org/10.1007/s11214-016-0245-4

Pritchett, P. L. (2001). Collisionless magnetic reconnection in a three-dimensional open system. *Journal of Geophysical Research*, *106*(A11), 25961–25977. https://doi.org/10.1029/2001JA000016

Pritchett, P. L. (2006a). Relativistic electron production during driven magnetic reconnection. *Geophysical Research Letters*, *33*(13), L13104. https://doi.org/10.1029/2005GL025267

Pritchett, P. L. (2006b). Relativistic electron production during guide field magnetic reconnection. *Journal of Geophysical Research*, *111*(A10), A10212. https://doi.org/10.1029/2006JA011793

Retinò, A., Vaivads, A., André, M., Sahraoui, F., Khotyaintsev, Y., Pickett, J. S., et al. (2006). Structure of the separatrix region close to a magnetic reconnection X-line: Cluster observations. *Geophysical Research Letters*, *33*(6), L06101. https://doi.org/10.1029/2005GL024650

Russell, C. T., Anderson, B. J., Baumjohann, W., Bromund, K. R., Dearborn, D., Fischer, D., et al. (2016). The magnetospheric multiscale magnetometers. *Space Science Reviews*, *199*(1–4), 189–256. https://doi.org/10.1007/s11214-014-0057-3

Sonnerup, B. U. Ö. (1979). Magnetic field reconnection. In L. T. Lanzerotti, C. F. Kennel, & E. N. Parker (Eds.), *Solar system plasma physics* (Vol. 3, pp. 45–108). North-Holland.

Su, Y., Veronig, A., Holman, G., Dennis, B. R., Wang, T., Temmer, M., & Gan, W. (2013). Imaging coronal magnetic-field reconnection in a solar flare. *Nature Physics*, *9*(7), 489–493. https://doi.org/10.1038/nphys2675

Terasawa, T. (1983). Hall current effect on tearing mode instability. *Geophysical Research Letters*, *10*(6), 475–478. https://doi.org/10.1029/GL010i006p00475

Torbert, R. B., Burch, J. L., Phan, T. D., Hesse, M., Argall, M. R., Shuster, J., et al. (2018). Electron-scale dynamics of the diffusion region during symmetric magnetic reconnection in space. *Science*, *362*(6411), 1391–1395. https://doi.org/10.1126/science.aat2998

Turner, D. L., Cohen, I. J., Bingham, S. T., Stephens, G. K., Sitnov, M. I., Mauk, B. H., et al. (2021). Characteristics of energetic electrons near active magnetotail reconnection sites: Tracers of a complex magnetic topology and evidence of localized acceleration. *Geophysical Research Letters*, *48*(2), e2020GL090089. https://doi.org/10.1029/2020GL09008

Wang, H., Lu, Q., Huang, C., & Wang, S. (2016). The mechanisms of electron acceleration during multiple X line magnetic reconnection with a guide field. *The Astrophysical Journal*, *821*(2), 84. https://doi.org/10.3847/0004-637X/821/2/84

Wang, R., Cheng, Z., Slavin, J. A., Lu, Q., Raines, J., Lu, S., et al. (2024). Direct detection of ongoing magnetic reconnection at Mercury's high-latitude magnetopause. *Geophysical Research Letters*, *51*(5), e2023GL106282. https://doi.org/10.1029/2023GL106282

Wang, R., Du, A., Nakamura, R., Lu, Q., Khotyaintsev, Y. V., Volwerk, M., et al. (2013). Observation of multiple sub-cavities adjacent to single separatrix. *Geophysical Research Letters*, *40*(11), 2511–2517. https://doi.org/10.1002/grl.50537

Wang, R., Lu, Q., Du, A., & Wang, S. (2010). In situ observations of a secondary magnetic island in an ion diffusion region and associated energetic electrons. *Physical Review Letters*, *104*(17), 175003. https://doi.org/10.1103/PhysRevLett.104.175003

Wang, R., Lu, Q., Huang, C., & Wang, S. (2010). Multispacecraft observation of electron pitch angle distributions in magnetotail reconnection. *Journal of Geophysical Research*, *115*(A1), A01209. https://doi.org/10.1029/2009JA014553

Wang, R., Lu, Q., Khotyaintsev, Y. V., Volwerk, M., Du, A., Nakamura, R., et al. (2014). Observation of double layer in the separatrix region during magnetic reconnection. *Geophysical Research Letters*, *41*(14), 4851–4858. https://doi.org/10.1002/2014GL061157

Wang, R., Lu, Q., Li, X., Huang, C., & Wang, S. (2010). Observations of energetic electrons up to 200 keV associated with a secondary island near the center of an ion diffusion region: A cluster case study. *Journal of Geophysical Research*, *115*(A11), A11201. https://doi.org/10.1029/2010JA015473

Wang, R., Lu, Q., Nakamura, R., Huang, C., Du, A., Guo, F., et al. (2016). Coalescence of magnetic flux ropes in the ion diffusion region of magnetic reconnection. *Nature Physics*, *12*(3), 263–267. https://doi.org/10.1038/nphys3578

Xiong, Q. Y., Huang, S. Y., Yuan, Z. G., Jiang, K., Xu, S. B., Wei, Y. Y., et al. (2022). Statistic properties of electron energy enhancement during the inner electron diffusion region crossing. *Journal of Geophysical Research: Space Physics*, *127*(10), e2022JA030760. https://doi.org/10.1029/2022JA030760

Yu, X., Lu, Q., Wang, R., Gao, X., Sang, L., & Wang, S. (2021). Simultaneous observation of whistler waves and electron cyclotron harmonic waves in the separatrix region of magnetopause reconnection. *Journal of Geophysical Research: Space Physics*, *126*(10), e2021JA029609. https://doi.org/10.1029/2021JA029609

Yu, X., Lu, Q., Wang, R., Huang, K., Gao, X., & Wang, S. (2021). MMS observations of broadband electrostatic waves in electron diffusion region of magnetotail reconnection. *Journal of Geophysical Research: Space Physics*, *126*(3), e2020JA028882. https://doi.org/10.1029/2020JA028882

Yu, X., Wang, R., Lu, Q., Russell, C. T., & Wang, S. (2019). Nonideal electric field observed in the separatrix region of a magnetotail reconnection event. *Geophysical Research Letters*, *46*(19), 10744–10753. https://doi.org/10.1029/2019GL082538

Zelenyi, L. M., Lominadze, J. G., & Taktakishvili, A. L. (1990). Generation of the energetic proton and electron bursts in planetary magnetotails. *Journal of Geophysical Research*, *95*(A4), 3883–3891. https://doi.org/10.1029/JA095iA04p03883